Langmuir

Article

pubs.acs.org/Langmuir

Raman Spectroscopy Insights into the Size-Induced Structural Transformation in SnSe Nanolayers

Michael Ludemann,[†] Ovidiu D. Gordan,[†] Dietrich R. T. Zahn,*[,†] Matt Beekman,[‡] Ryan Atkins,[§] and David C. Johnson*[,§]

[†]Semiconductor Physics, Technische Universität Chemnitz, D-09107 Chemnitz, Germany

[‡]Department of Natural Sciences, Oregon Institute of Technology, Klamath Falls, Oregon 97601, United States

[§]Department of Chemistry and Materials Science Institute, University of Oregon, Eugene, Oregon 97403, United States

ABSTRACT: Raman spectroscopy is used to probe the structural changes in $[SnSe]_m[MoSe_2]_n$ ferecrystal thin films as a function of m, the number of bilayers of SnSe. In spite of the interleaved structure in the intergrowths, Raman spectra can be described as a superposition of spectra from the individual components, indicating that the interaction at the interface between the components is relatively weak. Analysis of room-temperature Raman spectra indicate that the $MoSe_2$ layers separating the SnSe layers are nanocrystalline in all of the samples studied, with little change as the number of Se−Mo−Se trilayers (n) or SnSe bilayers (m) increases, reflecting the rotational disorder between adjacent trilayers. A thickness-dependent, continuous transition occurs in the SnSe layer as m is increased, from a pseudotetragonal structure when the layers are thin to a bulk-like orthorhombic SnSe structure when the SnSe layer thickness is increased. Polarization analysis of the Raman scattering from these materials allows the symmetry evolution of the SnSe layers through this transition to be determined.

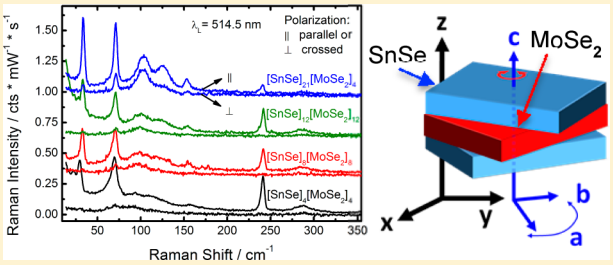

1. INTRODUCTION

Preparation of ultrathin two-dimensional layers of materials, especially those without epitaxial relationships to either substrate or capping layers and those that are fragments of three-dimensional structures, is the current focus of intense efforts, being driven by the expectation of extraordinary properties, new phenomena, and commercial applications.[1−4] Stacking such two-dimensional building blocks of different materials in designed sequences creates additional opportunities for many applications by taking advantage of unique combinations of electrical and optical properties found in the building blocks.[5,6] In addition to the potentially unique properties of the individual ultrathin building blocks, the interface between two dissimilar crystalline materials provides a unique bonding environment for atoms and another tool for creating novel structures, properties, and devices.[7−10] A particular challenge in this research is characterizing the structure of the two-dimensional layers, as traditional approaches such as X-ray diffraction, X-ray reflectometry, and electron microscopy become more challenging as thickness decreases and there is no epitaxial relationship between substrate and the structure of interest. The challenges are similar to detecting surface distortions in nanoparticles when the lack of a regular array of nanoparticles limits the ability of diffraction techniques to detect the interface structure.[11−13]

Recently, we reported a systematic change in in-plane lattice parameters of SnSe from square to rectangular in $[(SnSe)_{1.04}]_m(MoSe_2)_n$ ferecrystals (a turbostratically disordered polymorph of a misfit layered compound, see Figure 1) as m, the thickness of the SnSe layer, was increased,[14] which mimics the continuous structural phase transition that occurs in SnSe as temperature is decreased. These compounds lack an epitaxial relationship between the layers, resulting in independent 2-D layers without strain-induced defects such as dislocations.[15] While the lack of an epitaxial relationship between constituents in these compounds allows intrinsically size-induced effects to be delineated from strain effects in materials with well-defined nanostructure, the lack of distinct (hkl) $(h, k \neq 0; l \neq 0)$ reflections originating from the overall intergrowth and the large degree of diffuse scattering originating from the turbostratic disorder presents significant challenges to the determination of the three-dimensional structure of the two independent constituent structures as well as the relationship between them.

Various phase transitions have been observed in Group IV chalcogenide compounds under the influence of temperature,[16−19] pressure,[20,21] or interface strain.[22] As bulk crystals, SnSe exists in two modifications, e.g., the orthorhombic GeS-type α-phase (D_{2h}^{16} and $Pnma(/Pcmn/Pbnm)$) and the "pseudotetragonal orthorhombic" TlI-type β-phase modification (D_2^{17} and $Cmcm$), respectively.[16] With increasing temperature, the lattice parameters of the short axes (a and b) approach each other and become indistinguishable at 807 K.[17] The long axis parameter c increases continuously but "does

Received: May 12, 2014
Revised: June 16, 2014
Published: June 18, 2014

   dx.doi.org/10.1021/la501722d | Langmuir 2014, 30, 8209−8214

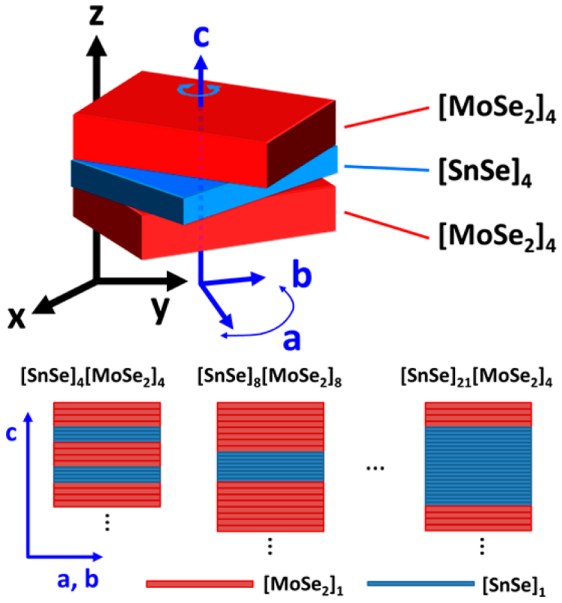

Figure 1. Sketch of the $[SnSe]_m[MoSe_2]_n$ turbostratically disordered mismatched layered samples. m and n represent the number of Se−Mo−Se trilayers and SnSe bilayers. Each Se−Mo−Se trilayer is 6.71 nm thick, and each SnSe bilayer is 5.81 nm thick.[32] The top figure attempts to show the rotational disorder between the SnSe and the $MoSe_2$ structural units. The rotational disorder between the $MoSe_2$ structural units within a single layer is not shown.

not reach the length corresponding to a transition to the NaCl-type structure" resulting in $a \approx b < c$.[16] A pressure-induced (room temperature) phase transition found for PbSe[18] and SnS[20] was not observed in the case of SnSe for pressures up to 36 GPa.[21] Nevertheless, cubic SnSe with a layer thickness of 100 nm was observed via epitaxial growth on NaCl substrates where the intrinsic stress is expected to be very small (~1 kbar),[22] and a cubic structure was found for $Pb_{2-x}Sn_xS_2$ nanocrystals[23] that is not stable in the bulk. The detailed relationships between the size-induced structural phase transition recently reported and the structural transition observed in the bulk material and isolated nanocrystals have yet to be established.

Raman and other spectroscopies are increasingly used as powerful tools for characterizing single slabs of two-dimensional materials.[24−26] In this work, we show that Raman spectroscopy is an elegant and efficient method to follow and identify structural changes in compounds containing stacks of two independent structural layers. The room-temperature data indicate that the $MoSe_2$ layers separating the SnSe layers are nanocrystalline and do not change as the thickness of the layer, n, increases. For SnSe, however, we observe a thickness-dependent, gradual transition from bulk-like orthorhombic SnSe layers when the SnSe layer thicknesses are large to a pseudotetragonal phase when the layers are thin. The thickness of SnSe appears to be the controlling factor, suggesting that the ratio of surface to volume free energy of the SnSe layers drives this structural change.[14]

2. EXPERIMENTAL SECTION

Modulated elemental reactant precursors were deposited on silicon substrates using a custom-built physical vapor deposition system.[27] Selenium was deposited using an effusion cell, while tin and molybdenum were deposited using electron beam guns. The thickness of each elemental layer was monitored using quartz crystal microbalances. The background pressure inside the chamber during film deposition was maintained between 7×10^{-8} and 7×10^{-7} mbar for all reported samples. A typical deposition consisted of repetitions of the layer sequence $n \times$ (Mo−Se) + $m \times$ (Sn−Se) which was repeated until a thin film of the desired thickness was obtained, typically 50−100 nm. The precursor was calibrated to contain an excess of 2% Se to account for evaporation loss during annealing. The thickness of each layer in the repeating sequence was calibrated via a method described previously such that each layer self-assembles into the targeted unit cell upon annealing.[28] Samples were annealed on a hot plate at 450 °C in a nitrogen atmosphere. Electron-probe microanalysis (EPMA) was used to confirm the composition of the thin film samples.[29] EPMA compositions were in agreement with the expected compositions, within experimental uncertainty.

The Raman spectrometer used was a Dilor XY triple monochromator with 800 mm focal length, 1800 lines/mm grating, operated in subtractive mode with an attached Peltier-cooled multichannel charge-coupled device (CCD) detector. In order to avoid low-frequency nitrogen rotational modes in the Raman spectra, samples were measured in a vacuum chamber optically coupled to the spectrometer. The spectral resolution of the spectrometer was 2.5 cm^{-1}. A Coherent Ar ion laser with a wavelength of 514.5 nm (2.41 eV) provided the excitation light. The scattered light was collected in backscattering geometry normal to the sample surface with a numerical aperture of 0.18. The applied laser power of less than 5 mW was focused on the samples inside the vacuum chamber to a rather large spot size of approximately 300 μm in diameter due to the low thermal conductivity of the samples.

3. RESULTS AND DISCUSSION

Raman spectra for four different $[SnSe]_m[MoSe_2]_n$ samples are presented in Figure 2. Qualitatively, the modes above ~240

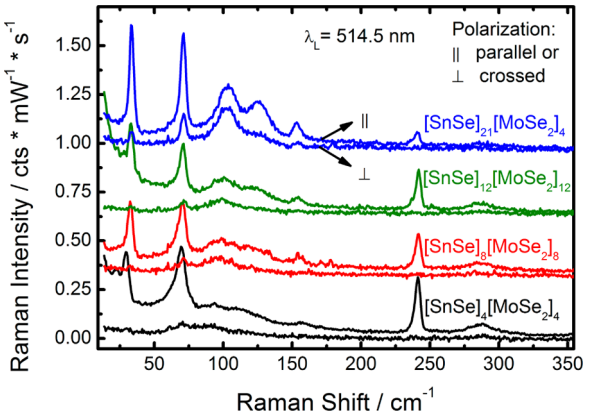

Figure 2. Raman spectra of four $[SnSe]_m[MoSe_2]_n$ samples.

cm^{-1} have lower relative intensities in the $[SnSe]_{21}[MoSe_2]_4$ sample than for the other $[SnSe]_m[MoSe_2]_m$ samples with approximately equal mole fractions of SnSe and $MoSe_2$, suggesting that the modes below 200 cm^{-1} can be assigned to SnSe and the modes above 200 cm^{-1} to $MoSe_2$. This interpretation is confirmed by comparison of the spectra of a $MoSe_2$ single-crystal foil with the turbostratically disordered $[SnSe]_m[MoSe_2]_n$ samples. As shown in Figure 3, the predominant vibrational mode of the $MoSe_2$ crystal at 243 cm^{-1} shifts to lower energy and becomes broader and more asymmetric in all of the $[SnSe]_m[MoSe_2]_n$ samples. For the $[MoSe_2]_4$ spacer layer, we do not observe any Davydov splitting due to the rotational disorder in the z direction. Any potential splitting would be relatively small and remain hidden within the width and asymmetry of the A_{1g} peak. Such behavior is usually observed when the crystal order or the grain size is decreased.[30]

dx.doi.org/10.1021/la501722d | Langmuir 2014, 30, 8209−8214

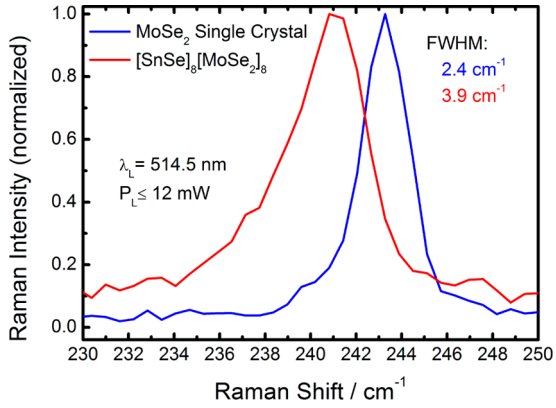

Figure 3. Raman spectra of a single crystal of $MoSe_2$ (blue) and a $[SnSe]_8[MoSe_2]_8$ sample annealed at 450 °C (red). Values of the full width at half-maximum (fwhm) for each sample are given on the right.

No vibrational modes for the $MoSe_2$ samples were observed below the mode at ~243 cm^{-1}, further evidence that all of the vibrational modes below this energy in Figure 2 result from modes of the SnSe constituent in the $[SnSe]_m[MoSe_2]_n$ samples. The positions of these modes below 200 cm^{-1} also agree well with the literature values reported for bulk SnSe, supporting this assertion.[31]

The ability to describe the Raman spectrum of the $[SnSe]_m[MoSe_2]_n$ layers as a superposition of spectra originating from the individual SnSe and $MoSe_2$ constituents suggests that the vibrational coupling between the layers is weak, consistent with previously reported X-ray diffraction studies.[32] In contrast to the vibrational modes assigned to $MoSe_2$ (~240 cm^{-1}) that do not change, the position, width, and shape of the vibrational modes of SnSe (below 200 cm^{-1}) change significantly as the SnSe layer thickness increases. Similarly, the in-plane *a*-axis lattice parameter of $MoSe_2$ does not vary as either *m* or *n* in $[SnSe]_m[MoSe_2]_n$ is varied but the in-plane *a*-axis and *b*-axis lattice parameters of the SnSe constituent vary considerably as *m* is varied as shown in Figure 4. The systematic change in lattice parameters of SnSe as a function of *m* in $[SnSe]_m[MoSe_2]_n$ is similar to what is observed when bulk SnSe undergoes a second-order phase transition as a function of temperature.[16]

Previous literature reports on bulk SnSe were used to assist in symmetry assignments to the modes below 200 cm^{-1}. At room temperature, bulk SnSe belongs to the *Pnma* (No. 62) space group (orthorhombic Bravais lattice) with the Sn and Se atoms in 4c Wyckoff positions (*x*, 1/4, *z*) and is expected to have 12 Raman-active vibrational modes, 4 A_g, 2 B_{1g}, 4 B_{2g}, and 2 B_{3g}, according to group theory. For a more detailed discussion on group theoretical considerations of SnSe see Chandrasekhar et al.[31] or Nikoli.[33] The Raman-active modes have Raman tensors with the following structure

$$A_g: \begin{pmatrix} d & 0 & 0 \\ 0 & e & 0 \\ 0 & 0 & f \end{pmatrix}; \quad B_{1g}: \begin{pmatrix} 0 & p & 0 \\ p & 0 & 0 \\ 0 & 0 & 0 \end{pmatrix};$$

$$B_{2g}: \begin{pmatrix} 0 & 0 & q \\ 0 & 0 & 0 \\ q & 0 & 0 \end{pmatrix}; \quad B_{3g}: \begin{pmatrix} 0 & 0 & 0 \\ 0 & 0 & r \\ 0 & r & 0 \end{pmatrix}$$

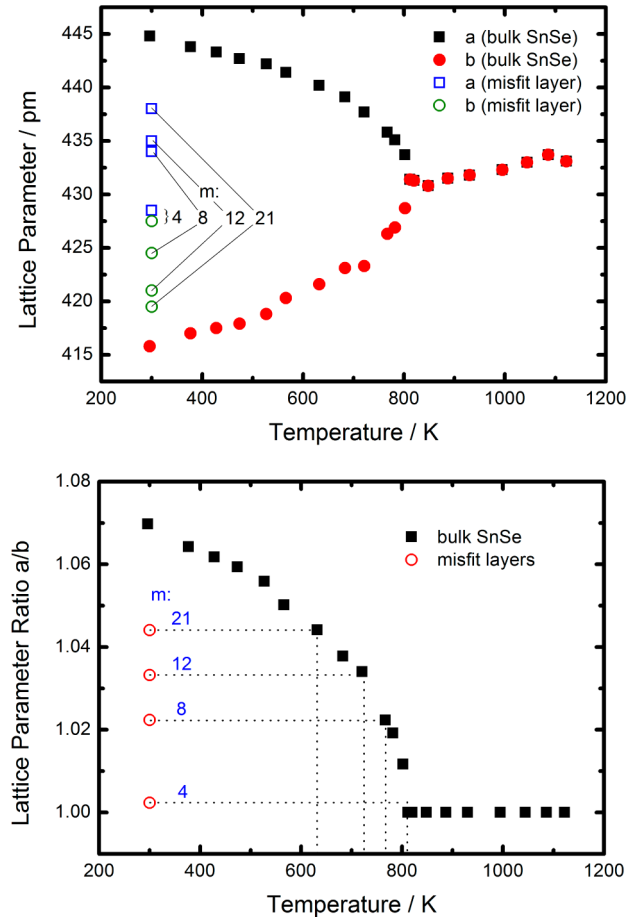

Figure 4. Temperature-dependent *a* and *b* lattice parameters of SnSe bulk material[21] are compared with the in-plane lattice parameters for the SnSe constituent in $[SnSe]_m[MoSe_2]_n$ as a function of *m*.

Hence, the Raman-active vibrational modes are visible only for particular orientations of the crystal axes with respect to the incident and collected laser light and its polarization. For bulk-like SnSe, the 4 A_g modes should be visible in the parallel configuration, while 2 B_{1g} should be visible in the crossed configuration. The B_{2g} and B_{3g} modes should not be visible in the applied measurement configuration, in which the excitation is incident along the axial direction of the highly aligned nanocrystals (cf. Figure 1).

Figure 5 contains our proposed assignments for the Raman modes seen in the $[SnSe]_{21}[MoSe_2]_4$ sample, assuming that the thickest layers can be assumed to be bulk like. The 4 A_g modes are observed in the parallel configuration, but only one B_{1g} mode could be resolved for crossed polarization. From the literature it is known that the other B_{1g} mode has a low intensity and is expected at 37 cm^{-1}.[31] Support for these assignments can be obtained by examining the Raman tensors for different modes in crossed and parallel configurations. For the sample with the most bulk-like SnSe layers, the observed B_{1g} mode at 103 cm^{-1} has almost the same intensity in crossed and parallel configuration. This can be explained as follows. If a bulk single crystal is rotated by 45° about the axial direction (*c* axis according to Figure 1), the Raman tensor of the B_{1g} mode transforms as follows

dx.doi.org/10.1021/la501722d | *Langmuir* 2014, 30, 8209−8214

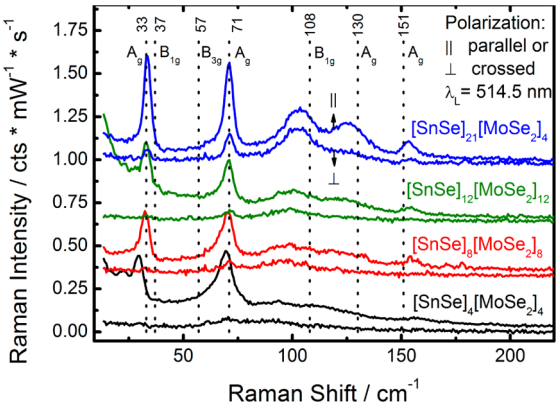

Figure 5. Raman spectra of $[SnSe]_m[MoSe_2]_n$ compounds in crossed $(-z(yx)z)$ and parallel $(-z(xx)z)$ configuration where the z axis is parallel to the c axis of the layer system and perpendicular to the layers. Dotted lines indicate the frequency of vibration of bulk SnSe with the corresponding symmetry assignment of Chandrasekhar.[31]

$$B_{1g}: \begin{pmatrix} 0 & p & 0 \\ p & 0 & 0 \\ 0 & 0 & 0 \end{pmatrix} \xrightarrow{\theta = 45^\circ} \begin{pmatrix} p & 0 & 0 \\ 0 & -p & 0 \\ 0 & 0 & 0 \end{pmatrix}$$

After the crystal rotation, the B_{1g} mode which was previously only observed in crossed configuration is now only visible in the parallel configuration. Therefore, the Raman signal in crossed and parallel configurations should be equal if the a and b axes of the individual SnSe layers are randomly oriented in the sample plane throughout the illuminated area. This agrees with the prior diffraction studies that the turbostratically disordered layers are parallel to the substrate and the c axis is perpendicular to the substrate. The experiment (see Figure 5) shows that the 4 Ag modes are much weaker but still visible for the crossed polarization. The Raman tensor of the Ag mode transforms as follows

$$A_g: \begin{pmatrix} d & 0 & 0 \\ 0 & e & 0 \\ 0 & 0 & f \end{pmatrix} \xrightarrow{\theta = 45^\circ} \begin{pmatrix} \frac{1}{2}d + \frac{1}{2}e & \frac{-1}{2}d + \frac{1}{2}e & 0 \\ \frac{-1}{2}d + \frac{1}{2}e & \frac{1}{2}d + \frac{1}{2}e & 0 \\ 0 & 0 & f \end{pmatrix}$$

If the tensor elements d and e have the same value, the off-diagonal elements (responsible for the intensity in crossed configuration) are canceled out, and the A_g modes are visible only in the parallel configuration. Taking into account the slightly visible A_g modes in crossed polarization, one concludes that the parameters d and e of the A_g Raman tensor are not exactly equal but must have similar values.

In Figure 5, five trends are observed with decreasing SnSe layer thickness. First, the intensity of the high-energy SnSe vibrational modes decreases until only 2 A_g modes remain. Second, the intensity of the A_g modes in crossed polarization almost completely vanishes. Third, all vibrational modes below 150 cm^{-1} shift to lower energies. Fourth, the width of the A_g modes increases, and fifth, there is an increasing shape asymmetry associated with the peaks. We first address the first two effects. A decrease in the number of vibrational modes is a strong indication of a transition to a crystal structure with a higher symmetry. This agrees with the X-ray diffraction study, which found the in-plane lattice parameters approach a common value as the thickness decreases.[14] The decrease in the intensity of the A_g modes in crossed polarization indicates that the Raman tensor of the A_g mode changes, with parameters d and e approaching the same value as shown below

$$A_g: \begin{pmatrix} d & 0 & 0 \\ 0 & d & 0 \\ 0 & 0 & f \end{pmatrix}$$

This change in the number of modes and in the A_g tensor allows us to rule out potential space groups for the SnSe layers as they become thinner. Bulk SnSe undergoes a transition from the α to the β phase as temperature is raised, and it is stated that the high-temperature phase is still orthorhombic ("pseudotetragonal") with the space group *Cmcm* (No. 63) and lattice parameters $a \approx b < c$.[16] If the thin SnSe layers in $(SnSe)_4(MoSe_2)_4$ had this space group, only 2 A_g modes would be expected, in agreement with the data in Figure 5. Contrary to the experiment, however, two B_{1g} modes should also be visible. The *Cmcm* space group also does not explain the vanishing Ag modes in crossed polarization, because the A_g Raman tensor of the *Cmcm* space group has exactly the same structure as in the *Pnma* case. Therefore, the thin SnSe layers cannot have a structure described by the *Cmcm* space group.

The changes in the Raman spectra with decreasing SnSe layer thickness is consistent with a phase transition from an orthorhombic (*Pnma*) to a tetragonal Bravais lattice. A tetragonal Bravais lattice is consistent with the observed reduction in the number of vibrational modes as the layers become thin. The selection rules for the B_{1g} mode also change in going from orthorhombic to tetragonal Bravais lattice such that no mode would be expected in crossed polarization for the given measurement configuration because the first two diagonal elements of the corresponding Raman tensor of the A_g modes have the same value in a tetragonal Bravais lattice (structure d, d, f). Diffraction experiments are also consistent with a tetragonal Bravais lattice, as the observed a and b lattice parameters in $[SnSe]_4[MoSe_2]_4$ are equal within experimental uncertainty.[14] While the Raman data do not provide us with enough information to identify the specific space group, it yields confidence that the space group is tetragonal.

The three additional trends in the Raman spectra with decreasing SnSe layer thickness allow us to make additional important inferences into the nature of the structure of the SnSe nanolayers. As the mass of the Sn and Se atoms does not change with the layer thickness, the shift to lower wavenumbers could be explained by either longer distances between the atoms indicating weaker bonding or a broadening of the distribution of bond lengths and/or angles. Figure 4 shows that the lattice parameter b increases while parameter a decreases as the layer thickness decreases. Presuming the thin SnSe layers are undergoing a similar structural transition to that which occurs at high temperatures in the bulk compound, the unification of the lattice parameters a and b is accompanied by a significant increase in the two Sn−Se in-plane bonding distances and anomalous increases in the in-plane elements of the atomic displacement tensor U_{ij} as the Sn atoms transition from 3 + 2 coordination by Se to 4 + 1 coordination.[16−19] Therefore, it is expected that the vibrations should shift to lower frequencies with decreasing SnSe layer thickness, which is in good agreement with the observed trends in the measurements.

dx.doi.org/10.1021/la501722d | *Langmuir* 2014, 30, 8209−8214

As presented in Figure 3, similar behavior concerning shift, width, and asymmetry of the Raman peaks measured from thin SnSe is observed for $MoSe_2$ (relative to the bulk spectrum), although in this case there is no evidence that a structural transition occurs with decreased domain size.[14] Specifically, the vibrational mode of turbostratically disordered $MoSe_2$ layers in the $[SnSe]_m[MoSe_2]_n$ compounds are shifted to lower wavenumbers with respect to the $MoSe_2$ single crystal. Furthermore, the full width at half-maximum and the shape asymmetry are also seen to be higher than that reported for a single crystal. For SnSe, the width and asymmetry of the SnSe modes increases with decreasing layer thickness, suggesting a broadening of the distribution of atomic positions in the lattice. As discussed above, the composite nature of the Raman spectra indicates that the coupling between the layers at the SnSe–$MoSe_2$ interfaces is relatively weak. Due to the nature of the nonepitaxial interface between the two distinct structures, it is expected that the interfacial Sn and Se atoms exhibit a distribution of static displacements from the average structure as a result of the weak interaction with the neighboring $MoSe_2$ layer and minimization of the configurational free energy. In the case of conventional crystalline misfit layered compounds, superspace crystallography has been used to describe the structural modulation of atomic positions that is induced by interaction of the intergrowth components along the incommensurate direction(s).[34] In our SnSe–$MoSe_2$ films, further complexity is added by the presence of turbostratic disorder. As the layer thickness decreases, a greater fraction of the atoms are interfacial and the average deviation from the average structure likely increases. The broadening and red shift of the Raman peaks are both consistent with these notions. An additional possibility is that confinement becomes relevant because these layers have a thickness of only a few nanometers. This effect is known from semiconductor quantum wells, nanoparticles, or microcrystalline samples where Raman spectroscopy starts to probe higher k values of the phonon dispersion curve due to the lifting of the quasi momentum conservation rule. The asymmetrical shape of the vibrational modes with the pronounced tail toward the low-frequency side indicates that the frequencies of the optical branch of the phonon dispersion curve decrease with higher k values in the vicinity of the Γ point of the first Brillouin zone.

4. CONCLUSIONS

Vibrational spectroscopy is a valuable technique to probe for structural changes as a function of layer thickness and provide information about the potential symmetries of the respective constituent layers and can be used to quickly determine the range of m and n over which diffraction experiments would be most interesting. Turbostratically disordered $[SnSe]_m[MoSe_2]_n$ compounds with different layer thickness (m and n) were investigated with polarization-dependent Raman spectroscopy. While the Raman modes of $MoSe_2$ do not change as a function of layer thickness (n), Raman selection rules are consistent with SnSe undergoing a phase transition from an orthorhombic (*Pnma*) to a tetragonal Bravais lattice structure with decreasing layer thickness. This agrees with previous X-ray diffraction measurements, which show that the a and b lattice constants converge as m is decreased. Shifts of the vibrational modes to lower wavenumber and a broadening of the modes lead to the conclusion that the degree of internal structural disorder within the SnSe layers increases as layer thickness (m) decreases. The crystallinity of the $MoSe_2$ layers (annealed at 450 °C) is independent of the layer thickness, but it is lower than for $MoSe_2$ single crystals.

AUTHOR INFORMATION

Corresponding Authors

*E-mail: zahn@physik.tu-chemnitz.de.

*E-mail: davej@uoregon.edu.

Author Contributions

The manuscript was written through contributions of all authors.

Notes

The authors declare no competing financial interest.

ACKNOWLEDGMENTS

M.L., O.G., and D.R.T.Z. thank the German Research Foundation (DFG) International Research Training Group of Materials and Concepts for Advanced Interconnects and Nanosystems (GRK 1215) for financial support. R.A., M.B., and D.C.J. acknowledge support from the National Science Foundation through CCI grant number CHE-1102637.

REFERENCES

(1) Wang, Q. H.; Kalantar-Zadeh, K.; Kis, A.; Coleman, J. N.; Strano, M.S. Electronics and optoelectronics of two-dimensional transition metal dichalcogenides. *Nat. Nanotechnol.* **2012**, *7*, 699–712.

(2) Ghatak, S.; Pal, A. N.; Ghosh, A. Nature of Electronic States in Atomically Thin MoS_2 Field-Effect Transistors. *ACS Nano* **2011**, *5*, 7707–7712.

(3) Radisavljevic, B.; Radenovic, A.; Brivio, J.; Giacometti, V.; Kis, A. Single-layer MoS_2 transistors. *Nat. Nanotechnol.* **2011**, *6*, 147–150.

(4) Kang, J.; Tongay, S.; Zhou, J.; Li, J.; Wu, J. Band offsets and heterostructures of two-dimensional semiconductors. *Appl. Phys. Lett.* **2013**, *102*, 012111.

(5) Bertolazzi, S.; Krasnozhon, D.; Kis, A. Nonvolatile Memory Cells Based on MoS_2/Graphene Heterostructures. *ACS Nano* **2013**, *7*, 3246–3252.

(6) Sofos, M.; Goldberger, J.; Stone, D. A.; Allen, J. E.; Ma, Q.; Herman, D. J.; Tsai, W. W.; Lauhon, L. J.; Stupp, S. I. A synergistic assembly of nanoscale lamellar photoconductor hybrids. *Nat. Mater.* **2009**, *8*, 68–75.

(7) Breckenfeld, E.; Bronn, N.; Karthik, J.; Damodaran, A. R.; Lee, S.; Mason, N.; Martin, L. W. Effect of Growth Induced (Non)-Stoichiometry on Interfacial Conductance in La–lO_3/$SrTiO_3$. *Phys. Rev. Lett.* **2013**, *110*, 196804.

(8) Granozio, F. M.; Koster, G.; Rijnders, G. Functional Oxide Interfaces. *MRS Bull.* **2013**, *38*, 1017–1023.

(9) Hilgenkamp, H. Novel transport phenomena at complex oxide interfaces. *MRS Bull.* **2013**, *38*, 1026.

(10) Dawber, M.; Bousquet, E. New developments in artificially layered ferroelectric oxide superlattices. *MRS Bull.* **2013**, *38*, 1048.

(11) Shevchenko, E. V.; Talapin, D. V.; Kotov, N. A.; O'Brien, S.; Murray, C. B. Structural diversity in binary nanoparticle superlattices. *Nature* **2006**, *439*, 55–59.

(12) Talapin, D. V.; Shevchenko, E. V.; Bodnarchuk, M. I.; Ye, X. C.; Chen, J.; Murray, C. B. Quasicrystalline order in self-assembled binary nanoparticle superlattices. *Nature* **2009**, *461*, 964–967.

(13) Brown, L. O.; Hutchison, J. E. Formation and Electron Diffraction Studies of Ordered 2-D and 3-D Superlattices of Amine-Stabilized Gold Nanocrystals. *J. Phys. Chem. B* **2001**, *105*, 8911–8916.

(14) Beekman, M.; Disch, S.; Rouvimov, S.; Kasinathan, D.; Koepernik, K.; Rosner, H.; Zschack, P.; Neumann, W. S.; Johnson, D. C. Controlling Size-Induced Phase Transformations Using Chemically Designed Nanolaminates. *Angew. Chem., Int. Ed.* **2013**, *52*, 13211–13214.

(15) Heideman, C. L.; Tepfer, S.; Lin, Q.; Rostek, R.; Zschack, P.; Anderson, M. D.; Anderson, I. M.; Johnson, D. C. Designed Synthesis,

Structure, and Properties of a Family of Ferecrystalline Compounds $[(PbSe)_{1.00}]_m(MoSe_2)_n$. *J. Am. Chem. Soc.* **2013**, *135*, 11055−11062.
(16) Wiedemeier, H.; Csillag, F. J. The thermal expansion and high temperature transformation of SnS and SnSe. *Z. Kristallogr.* **1979**, *149*, 17−29.
(17) von Schnering, H. G.; Wiedemeier, H. The high temperature structure of β-SnS and β-SnSe and the B16-to-B33 type λ-transition path. *Z. Kristallogr.* **1981**, *156*, 143−150.
(18) Chattopadhyay, T.; Werner, A.; von Schnering, H. G.; Pannetier, J. Temperature and pressure induced phase transition in IV-VI compounds. *Rev. Phys. Appl.* **1984**, *19*, 807−813.
(19) Chattopadhyay, T.; Pannetier, J.; von Schnering, H. G. Neutron diffraction study of the structural phase transition in SnS and SnSe. *J. Phys. Chem. Solids* **1986**, *47*, 879−885.
(20) Ehm, L.; Knorr, K.; Dera, P.; Krimmel, A.; Bouvier, P.; Mezouar, M. Pressure-induced structural phase transition in the IV−VI semiconductor SnS. *J. Phys.: Condens. Matter* **2004**, *16*, 3545−3554.
(21) Leger, J. M.; Redon, A. M. Phase transformations and volume of the IV-VI GeTe semiconductor under high pressure. *J. Phys.: Condens. Matter* **1990**, *2*, 5655−5662.
(22) Mariano, A. N.; Chopra, K. L. Polymorphism in Some IV-VI Compounds Induced By High Pressure and Thin-Film Epitaxial Growth. *Appl. Phys. Lett.* **1967**, *10*, 282.
(23) Soriano, R. B.; Milliakas, C. D.; Wu, J.; Kanatzidis, M. G. Cubic form of $Pb_{2-x}Sn_xS_2$ stabilized through size reduction to the nanoscale. *J. Am. Chem. Soc.* **2012**, *134*, 3228−3233.
(24) Ferrari, A. C.; Meyer, J. C.; Scardaci, V.; Casiraghi, C.; Lazzeri, M.; Mauri, F.; Piscanec, S.; Jiang, D.; Novoselov, K. S.; Roth, S.; Geim, A. K. Raman Spectrum of Graphene and Graphene Layers. *Phys. Rev. Lett.* **2006**, *97*, 187401.
(25) Hajiyev, P.; Cong, C. X.; Qiu, C. Y.; Yu, T. Contrast and Raman spectroscopy study of single- and few-layered charge density wave material: 2H-$TaSe_2$. *Sci. Rep.* **2013**, *3*, 2593 DOI: 10.1038/srep02593.
(26) Chen, Y.; Dumcenco, D. O.; Zhu, Y.; Zhang, X.; Mao, N.; Feng, Q.; Zhang, M.; Zhang, J.; Tan, P. H.; Huang, Y.; Xie, L. Composition-dependent Raman modes of $Mo_{1-x}W_xS_2$ monolayer alloys. *Nanoscale* **2014**, DOI: 10.1039/C3NR05630A.
(27) Fister, L.; Li, X. M.; McConnell, J.; Novet, T.; Johnson, D. C. Deposition system for the synthesis of modulated, ultrathin-film composites. *J. Vac. Sci. Technol. A* **1993**, *11*, 3014−3019.
(28) Atkins, R.; Wilson, J.; Zschack, P.; Grosse, C.; Neumann, W.; Johnson, D. C. Synthesis of $[(SnSe)_{1.15}]_m(TaSe_2)_n$ Ferecrystals: Structurally Tunable Metallic Compounds. *Chem. Mater.* **2012**, *24*, 4594−4599.
(29) Phung, T. M.; Jensen, J.; Johnson, D. C.; Donovan, J. J.; McBurnett, B. G. Determination of the composition of Ultra-thin Ni-Si films on Si: constrained modeling of electron probe microanalysis and x-ray reflectivity data. *X-Ray Spectrom.* **2008**, *37*, 608−614.
(30) Tonndorf, P.; Schmidt, R.; Böttger, P.; Zhang, X.; Börner, J.; Liebig, A.; Albrecht, M.; Kloc, C.; Gordan, O.; Zahn, D. R. T.; de Vasconcellos, S. M.; Bratschitsch, R. Photoluminescence emission and Raman response of monolayer MoS_2, $MoSe_2$, and WSe_2. *Opt. Express* **2013**, *21*, 4908−4916.
(31) Chandrasekhar, H. R.; Humphreys, R. G.; Zwick, U.; Cardona, M. Infrared and Raman spectra of the IV-VI compounds SnS and SnSe. *Phys. Rev. B* **1977**, *15*, 2177−2183.
(32) Beekman, M.; Cogburn, G.; Heideman, C.; Rouvimov, S.; Zschack, P.; Neumann, W.; Johnson, D. C. New Layered Intergrowths in the Sn-Mo-Se System. *J. Electron. Mater.* **2012**, *41*, 1476−1480.
(33) Nikolić, P. M.; Milković, L.; Mihajlović, P.; Lavrenčić, B. Raman scattering in SnSe. *Czech. J. Phys. B* **1978**, *28*, 456−459.
(34) Wiegers, G. A. Misfit layer compounds: Structures and physical properties. *Prog. Solid State Chem.* **1996**, *24*, 1−139.